Preparation and Characterization of *Racomitrium japonicum* Moss Biochar and Its Adsorption of Sr(II)

Yang Yang,[a,#] Zijie Cheng,[a,#] Yufan Luo,[a] Xinran Li,[d] Yanbao Lei,[b] Anđelka Plenković-Moraj,[c] and Ke Chen [a,b,*]

Biochar is recognized as an effective sorbent for environmental management and many other applications. Herein the authors report biochar derived from moss *Racomitrium japonicum* L., prepared *via* pyrolysis at 400 °C to 1000 °C. The biochar was characterized by thermal gravimetric analysis (TGA), elemental analysis, Fourier-transform infrared spectroscopy (FT-IR), scanning electron microscopy (SEM), and X-ray photoelectron spectroscopy diffraction (XPS), as well as the ability to remove Sr^{2+} from aqueous solutions. The results indicated that a biochar with high thermal stability, specific surface area, and dense and mesoporous pores was obtained, with surface functional groups enhancing the adsorption process. Equilibrium adsorption data were consistent with the Langmuir isotherm model, indicating surface homogeneity, with maximum Sr^{2+} adsorption capacity of 225 mg/g at 25 °C. These results demonstrate that the *R. japonicum* moss biochar can be used to develop an efficient adsorbent for the removal of Sr (II) from aqueous solution and suggests its utility for further application in removing heavy metals from water.

DOI: 10.15376/biores.17.3.3965-3983

Keywords: Moss; Biochar; Sr^{2+}; Adsorption; Racomitrium japonicum L.

*Contact information: a: School of Life Science and Engineering, Southwest University of Science and Technology, Mianyang 621010, China; b: CAS Key Laboratory of Mountain Ecological Restoration and Bioresource Utilization & Ecological Restoration and Biodiversity Conservation Key Laboratory of Sichuan Province & China-Croatia "Belt and Road" Joint Laboratory on Biodiversity and Ecosystem Services, Chengdu Institute of Biology, Chinese Academy of Sciences, Chengdu, 610041, China; c: Department of Biology, Faculty of Science, University of Zagreb, Rooseveltov trg 6, 10000, Zagreb, Croatia; d: Department of Biology, Shenzhen MSU-BIT University, Shenzhen 518172, China; #: These authors contributed equally; *Corresponding author: chenke@swust.edu.cn*

INTRODUCTION

Bryophyte is one of the most abundant species on the earth's surface, covering 3% of the earth's surface. Due to the special cellular structure, mosses can grow in different extreme environments (Adamo *et al.* 2003; Yoshikawa *et al.* 2004). Therefore, it is also widely used to monitor trace metal pollution in the atmosphere (Stanković *et al.* 2018). Compared with other biomasses, moss has a high composition of sugars, cellulose, carbohydrates, and amino acids; its cellulose fibrils are 5 to 20 nm in width and could be observed directly on the cell wall of moss (Wyatt *et al.* 2008). In addition, the presence of lignin in moss has not been confirmed in previous studies (Espiñeira *et al.* 2011), all of which are preconditions for the preparation of applicable biochar. In previous studies, the cellulose content of moss was measured as 42.84% to 44.16% (Plank 1946), which is comparable to that of recent cellulosic biomass materials (Lawal *et al.* 2021). The current authors have roughly determined the cellulose content in *R. japonicum* L. at 33% to 36% using biochemical methods to ensure the minimum cellulose content in the material. In the application research of moss biomass, the *Sphagnum* is more common, which has been well evaluated in sewage treatment and electrochemical research, but research on other moss species is relatively scarce. It is necessary to strengthen the research and application of bryophytes, which are almost inexhaustible resources. The development and application of cellulose materials is conducive to solving the problems of high cost, harsh application conditions, and secondary environmental pollution in traditional sewage treatment methods (Llaurado 2011; Ly *et al.* 2019).

Biochar is an environmentally friendly adsorbent that can purify wastewater and air and can be used as a catalyst carrier (Alshameri *et al.* 2018; Xu *et al.* 2021; Yao *et al.* 2021). Biochar is usually produced by the slow pyrolysis of biomass in an inert gas atmosphere, resulting in physical and chemical changes with the degradation, dehydration, defatting, and aromatization of cellulose (Subratti *et al.* 2021). It contains abundant pore structures, including micropores, mesoporous pores, and macropores, and abundant functional groups are distributed on its surface (Li *et al.* 2021). Therefore, it has ideal adsorption and retention effect for different types of pollutants (Cha *et al.* 2016; Oliveira *et al.* 2017). Compared with lignin materials, cellulosic biochar often has a larger specific surface area and adsorption capacity and can produce a higher proportion of mesoporous structures (Deng *et al.* 2016). The single-cell structure of moss is more conducive to the formation of mesoporous structures of biochar. At the same time, biochar does not require complex activation processes, saving materials and reducing manufacturing costs, which is more in line with the concept of sustainable development. In selecting the preparation method of biochar, the traditional pyrolysis method will be helpful to optimize the final preparation process according to the actual results (Tripathi *et al.* 2016).

The increasingly serious effects of environmental pollution, such as the severe water shortage in many parts of the world, the rapid development of modern nuclear energy industry, and the imperfection of the production management system, are some of the reasons for this problem (Liu *et al.* 2021; Zamora-Ledezma *et al.* 2021). Sr(II), as a relatively new industrial element, has gradually come into view with the development of nuclear energy and the alloy industry, especially after the Chernobyl nuclear power plant leakage incident (1985, Ukraine) and Fukushima nuclear leakage incident (2011, Japan) (Steinhauser *et al.* 2014). Damage to organisms by Sr^{2+} is mainly due to the competitive behavior of Sr^{2+} toward Ca^{2+} (Burger and Lichtscheidl 2019), causing organ damage. Excessive accumulation of Sr(II) in the environment has significant toxicity to plants, inhibiting root growth and chlorosis (Nagata 2019). In the treatment of environmental heavy metal pollution, many works show that the adsorbent is an effective and economical method to solve these problems (Li *et al.* 2021). The aim of this work is to prepare biochar using readily available fibrous materials with some potential, to give some reference for the application of this material in pollution remediation and to provide a theoretical basis for future deep exploration.

EXPERIMENTAL

Preparation of Moss Biochar

The moss *R. japonic*um L. was cultivated and washed with deionized water to remove dust and impurities, then dried at 105 °C for 6 h, crushed, and filtered with a 0.45-

mm sieve. The biochar was prepared by filling a 120-mL capacity ark with 5 g of moss in a tubular furnace under nitrogen flow of 60 cm^3/min at different temperatures (400, 600, 800, and 1000 °C) and constant duration of heating (60 min, 90 min, and 120 min). The nitrogen flow rate of 40 to 70 cm^3/min was conducive to improving the mesoporous ratio of materials, which helps to adsorb and retain pollutants (Li *et al*. 2014). The moss biochar was labeled as SC. Each treatment included three replicates.

Characterization of Biomass and Biochar

A thermogravimetric analyzer (STA 449C; FNETZSCH-Gerätebau GmbH, Selb, Germany) was used to analyze the pyrolysis process of the material. Equations 1 and 2 were used to calculate the weight loss and yield of moss biochars. The morphology and structure of biomass and biochar were detected by scanning electron microscopy (SEM, Regulus 8100; Hitachi, Tokyo, Japan). A Fourier transform infrared spectrometer (Nicoet 460, Thermo Electron Corporation, Madison, WI, USA) was used to identify the carbon functional groups of biomass and biochar. Semi-quantitative characterization of C/O/N/S element content on the surface of the material was performed using X-ray photoelectron spectroscopy (XPS, Cermofield EscaLab 250Xi, Thermo Fisher Scientific, Waltham, MA, USA). Biochar was mixed with deionized water at a ratio of 1:20 and stirred at 150 rpm for 2 h at a constant speed. Values of pH and electrical conductance (EC) were determined using a pH electrode and an EC electrode. The cation exchange capacity (CEC) cation exchange capacity of biochar was determined by cobalt hexa-ammonia trichloride method:

$$\text{Weight loss} = Moss\ weight - Carbon\ weight \tag{1}$$

$$Yeid(\%) = \frac{Carbon\ weight}{Moss\ weight} \times 100\% \tag{2}$$

Adsorption of Sr(II) by Biochar

Reagents were purchased from Cologne Chemical Co., Ltd. (Chengdu, China) and were all analytically pure. The $SrCl_2$ was dissolved in deionized water to prepare the Sr(II) reserve solution with a concentration of 1000 mg/L. To prepare the working solution, the pH was modified to 2.0 ± 0.1 with 0.1 M HNO_3. The adsorption screening test was carried out for all biochar. 0.1 g biochar was added to 250 to 500 mg/L of working solution, and the biochar was filtered out after 24 h of continuous exposure at 25 °C. The Sr(II) residual concentration of the solution was measured, and the Sr(II) adsorption capacity of biochar was calculated with Eq. 2. For the kinetic test, 0.1 g biochar was added into 250 mL with 500 mg/L working solution, and then the solution concentrations were consecutively sampled and measured at 5, 10, 20, 40, 60, 90, 120, 150, 180, 360, 720, 1440, and 2880 min. In the isothermal experiment, 0.1 g of biochar was placed in 100 mL of working solution and adsorbed for 24 h. All adsorption was completed in a constant temperature shaker (25 °C, 120 rpm). The filtrate was filtered using a 0.45-μm microporous membrane and a disposable syringe and was diluted with 0.1 M of HNO_3. An atomic absorption spectrometer (AAS) acetylene flame method was used to determine Sr(II) in the diluted solution. The biochar adsorption quantity Q_t at t time was calculated with Eq. 2,

$$Q_t = (C_o - C_t) \times v / w \tag{3}$$

where C_o is the initial concentration (mg/L) of working liquid, V is the volume (L) of working liquid in the adsorption process, and W is the amount of biochar (mg).

Data Analysis

The significance of the test data was statistically analyzed using a one-way analysis of variance (ANOVA) in SPSS (26.0) software (SPSS Inc., Chicago, IL, USA), and the infrared data was analyzed by OMNIC software (Thermo Fisher Scientific, Waltham, MA, USA). All data were the mean and standard deviation obtained by replicating the test three times. The charts were drawn in Excel (2019) (Microsoft, Redman, WA, USA) and Origin (2019b) (OriginLab Corporation, Northhampton, MA, USA).

The Lagergren pseudo-first-order dynamics model and pseudo-second-order dynamics model were used to fit the dynamics data,

$$\log(q_e - q_t) = \log q_e - \frac{k_1}{2.303} \times t \tag{4}$$

$$\frac{t}{q_t} = \frac{1}{k_2 q_e^2} + \frac{t}{q_e} \tag{5}$$

where q_e is the adsorption amount (mg/g) on biochar adsorbent at adsorption equilibrium, q_t is the adsorption amount (mg/g) on biochar adsorbent at t min, k_1 and k_2 are rate constants of first-order and second-order kinetics, respectively.

Langmuir and Freundlich models were used to fit isothermal adsorption model:

$$q_\mathrm{e} = Q_\mathrm{max} \times \frac{K_\mathrm{L} C_\mathrm{e}}{1 + K_\mathrm{L} C_\mathrm{e}} \tag{6}$$

$$q_\mathrm{e} = K_\mathrm{F} {C_\mathrm{e}}^{1/\mathrm{n}} \tag{7}$$

In the Langmuir isothermal model, K_L is the affinity correlation coefficient between solute and adsorbent, C_e represents equilibrium concentration (mg/L), and Q_{max} is the maximum adsorption capacity (mg/g). According to the Freundlich isothermal model and the adsorption strength measurement, K_F is the predicted adsorption capacity (Ezzati 2020).

RESULTS AND DISCUSSION

Biochar Preparation, Properties, and Sr^{2+} Adsorption

The pyrolysis behavior curve (Fig. 1) was obtained by heating the moss from room temperature to 1000 °C at a heating rate of 10 °C/min in N_2 atmosphere. The thermogram showed the relationship between weight loss of the materials and temperature, water content, and ash content. When temperature rose to 105 °C, the weight loss of samples was mainly due to the evaporation of water (Kim *et al.* 2020). The weight loss trend of material pyrolysis increased from 220 °C, which was due to this temperature being the main degradation temperature range of cellulose and hemicellulose (Yiin *et al.* 2018; Saha *et al.* 2019). This trend was moderated by 352.5 °C, before which the organic compounds volatilized rapidly. At 687 °C, a relatively stable weight was obtained, which was attributed to the combustion consumption of fixed carbon in biochar and the decomposition of residual cellulose (Oginni and Tingi 2020). With the temperature rise, a series of reactions, such as decarboxylation and aromatization, are intensified in the carbonization process, and finally the ordered aromatic structure is formed, and the thermal decomposition is essentially completed (Anukam *et al.* 2015).

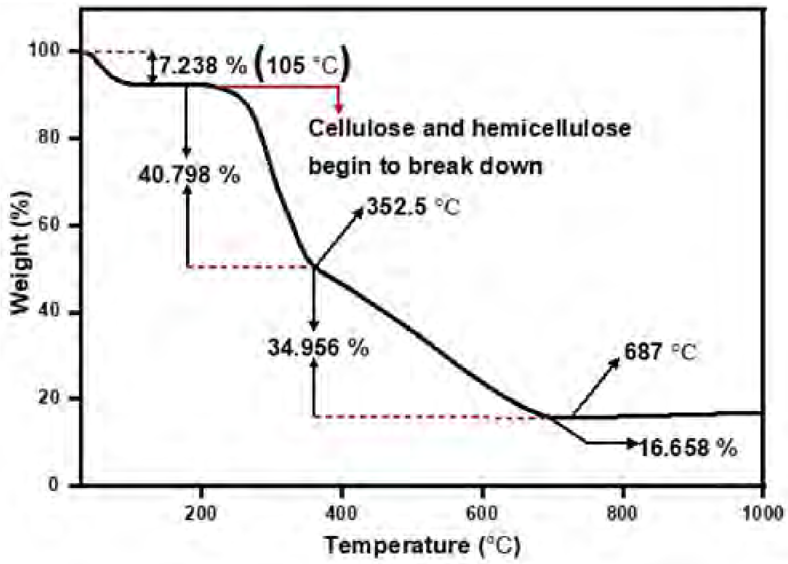

Fig. 1. Thermogravimetric analysis of moss biochar obtained from room temperature to 1000 °C

The results of weight loss and yield of samples at different temperatures and constant temperature time are shown in Table 1. Apparently, when the pyrolysis temperature increased from 400 to 1000 °C, the yield of biochar decreased from 47.66% to 17.2%, which was almost consistent with the lowest yield detected by the thermogravimetric analyzer (Fig. 1). The larger difference in yield between 400 and 600 ℃ as compared to 800 °C depended on the fact that most of the fixed carbon in the material below 600 °C had not been decomposed. In general, a higher carbonization temperature resulted in lower volatile content of the products because most of the non-carbon components in the biomass had been decomposed during the heating process. In the actual process of preparing biochar, the authors obtained a similar yield at higher temperature, because the increase in the amount of material requires a higher temperature to obtain similar products. In general, as the carbonization time increased, the yield decreased. A long time in a high- temperature environment makes the carbon component in the material completely burned, and the tar component in the material becomes volatilized. Further screening of these samples is needed to select the better sample group.

Table 1. Effect of Carbonization Conditions on Weight Loss of Sand Moss (*n*=3)

Carbonization Conditions		400 °C	600 °C	800 °C	1000 °C
60 min	Weight Loss (g)	2.62 ± 0.07	3.17 ± 0.02	3.54 ± 0.05	3.94 ± 0.03
	Yield (%)	47.66 ± 1.4	36.68 ± 0.46	29.16 ± 1.05	21.18 ± 0.65
90 min	Weight Loss (g)	2.82 ± 0.05	3.27 ± 0.02	3.69 ± 0.05	4.14 ± 0.02
	Yield (%)	43.59 ± 0.95	34.62 ± 0.48	26.13 ± 0.99	17.20 ± 0.38
120 min	Weight Loss (g)	2.88 ± 0.03	3.40 ± 0.03	3.85 ± 0.03	4.08 ± 0.11
	Yield (%)	42.44 ± 0.65	32.01 ± 0.62	23.01 ± 0.63	18.33 ± 2.23

Figure 2 shows the SEM images of moss biomass (S) and moss-derived biochars at different carbonization temperatures (400, 600, 800, and 1000 °C) for 90 min (labeled as SC400, SC600, SC800, and SC1000, respectively).

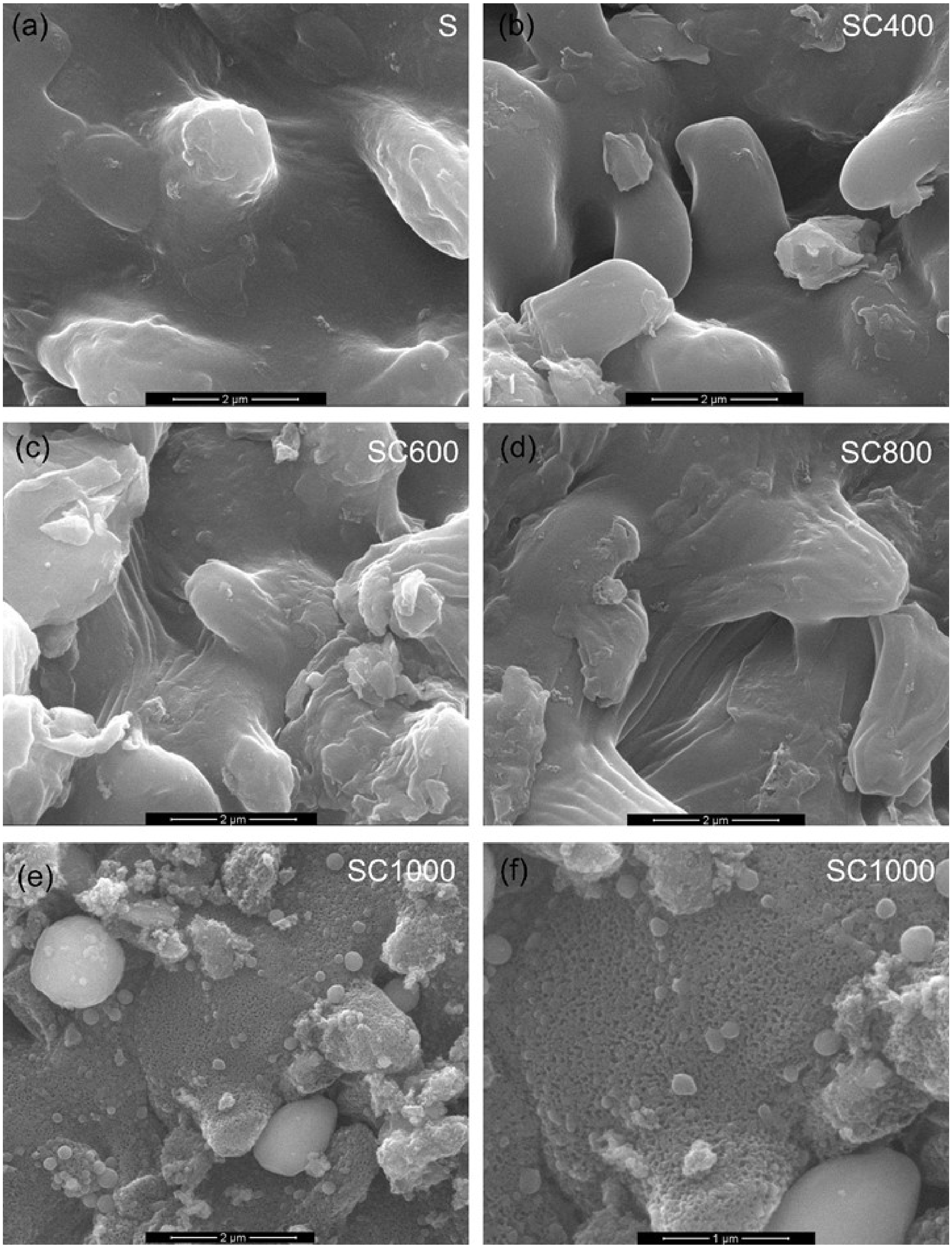

Fig. 2. SEM images of moss biomass (a) and moss-derived biochars at different carbonization temperatures for 90 min (b: SC400, c: SC600, d: SC800, and e: and f: SC1000)

The surface of the moss was smooth and dense (Fig. 2a), and the protrusion was a wart on the *R. japonic*um L. surface. Devolatilization, condensation, dehydration, and other reactions in the pyrolysis process at different temperatures will destroy the smooth surface structure of the moss to varying degrees, and the residual volatile components will be released. At the same time, the pores on the material surface obtained at higher temperatures were more dense and evenly distributed (Fig. 2e) (Saber *et al.* 2019). In Fig. 2f, the moss biochar obtained from *R. japonicum* L. at 1000 °C (SC1000) showed that the pore structure was intense, and the distribution and quantity of the holes played an important role in the adsorption reaction. The cellular pore distribution structure binds pollutants during the adsorption process and provides considerable space and channels for pollutants to pass through and stay. The smaller mesopores can serve as charge absorption binding sites, while ion transport is typically through larger mesopores.

It is a general biochar evaluation method to explore the adsorption capacity of materials to treat various pollutants in wastewater (Barquilha and Braga 2021). Because carbon atoms on the surface of biochar materials are easily oxidized in alkaline solution, thus weakening the electron-giving ability, the authors used 0.1 M HNO_3 to adjust the pH of the working solution to 2.0 ± 0.1. The authors tested the adsorption performance of all 36 biochar samples. As shown in Fig. 3, the biochar sample prepared at 1000 ℃ for 1.5 h showed satisfactory adsorption performance for Sr (II). This was largely due to the significant pore structure of moss carbon on the material surface under these conditions (Fig. 2f), and biochar produced at higher temperatures exhibits better adsorption properties because of its greater hydrophobicity (Choi *et al.* 2020).

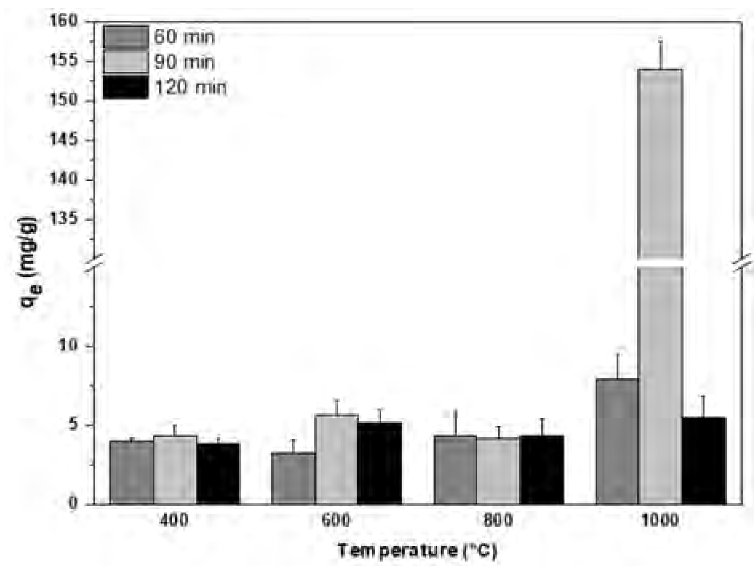

Fig. 3. Effect of carbonization temperature and time on Sr^{2+} adsorption by moss biochars; data presented are mean values with standard deviation (n = 3)

From the comprehensive assessment, the biochar specimens prepared at 1000 °C for 1.5 h were selected as representatives for further analysis, characterization, and exploration. In the BET measurement results, both BET surface area and pore volume at SC1000 increased significantly, and the pore size changed from 3.33 nm in the microporous range to 5.12 nm in the mesopore range. Combined with Fig. 2.e, it is believed that the pores on the surface of the material will develop well during the carbonization process at 1000 °C for 90 min.

Characterization of Moss Biomass and Biochar

Based on the adsorption ability of Sr^{2+}, the characterizations of SC1000 and the moss biomass (S) were compared to understand the adsorption mechanism. The pH of SC1000 was 11.11 (Table 2), indicating the decrease of hydroxyl oxygen-containing functional groups on the surface after high temperature carbonization (Zhang *et al.* 2015a), with the accumulation of alkali salts, such as carbonate and nitrate, on the surface (Zhang *et al.* 2015b; Jian *et al.* 2018). From Table 1, higher EC value and lower ash contents were found in SC1000, and the conductivity depended on the concentration of salt in the liquid. The biochar with higher ash content has higher salt content, resulting in higher electrical conductivity (Oginni and Tingi 2020). The increase of exchangeable cation content is more conducive to the adsorption and retention of organic matter. The specific surface area of biomass after high temperature carbonization increased significantly ($P < 0.05$) (Table 2), which was the result of chemical reaction caused by carbonization. It can be explained as the removal of volatile components in the carbonization process, which forms pores on the material surface. Moreover, the condensation degree of tar products decreased, and the core groups of phenolic OH, aromatic CO-, and aliphatic alkyl in the aromatic structure were removed (Oginni and Tingi 2020).

Table 2. Physicochemical Characteristics of moss biomass(S) and the moss biochar (SC1000)

	pH	EC (ms/cm)	CEC ($cmol^+/kg$)	BET Surface Area (m^2/g)	Pore Volume (cm^3/g)	Pore Size (nm)
S	6.83	0.28	24.676	74.4176	0.0618	3.3252
SC1000	11.11	3.25	161.38	277.5464	0.3554	5.1220

The FT-IR of biomass and the SC1000 after Sr(II) adsorption in the range of 400 to 4000 cm^{-1} with an energy resolution of 1 cm^{-1} are shown in Fig. 4. The method of infrared spectrum analysis and peak recognition of the material has been determined (Schwanninger *et al.* 2004; Reza *et al.* 2014). The absorbance peak of 3600 to 3200 cm^{-1} was the stretching of cellulose O-H, 2919 cm^{-1} corresponding aliphatic lipid chain ($-CH_3$), and the signal of the methyl group almost disappeared after carbonization (Saha *et al.* 2019). SC-Sr(II) showed C=O pull-up of the carboxyl group at 1740 to 1700 cm^{-1}, which is a characteristic functional group common in cellulose and hemicellulose materials. The sharp absorption peak of 1627 to 1639 cm^{-1} may correspond to the C=C (Jian *et al.* 2018), which is attributed to the stretching vibration of the aliphatic carbon bond, while the signal weakening in this range in SC1000 should be caused by the removal of hydrophilic hydrocarbon groups of cellulose or hemicellulose. The absorbance peak corresponding to 1420 to 1429 cm^{-1} should be the C-N bond, while the absorption peak corresponding to 1380 to 1389 cm^{-1} can be inferred to be C-H bending or C-N stretching (Kadam *et al.* 2019). The peak at 1259 cm^{-1} corresponds to O-H bending (Huff *et al.* 2014), while the absorbance peak at 1054 to 1069 cm^{-1} corresponds to the stretching of the C-O of the material, which can be attributed to alcohols, phenols, and carboxyl groups (Uchimiya *et al.* 2011). In addition, 780 cm^{-1} corresponds to C-H bond bending outside the aromatic plane. The results showed that the infrared spectrum of pyrolytic biochar was flatter than that of biomass, and most of the oxygen-containing functional groups were decomposed during pyrolysis, but some aromatic hydrocarbon groups were retained.

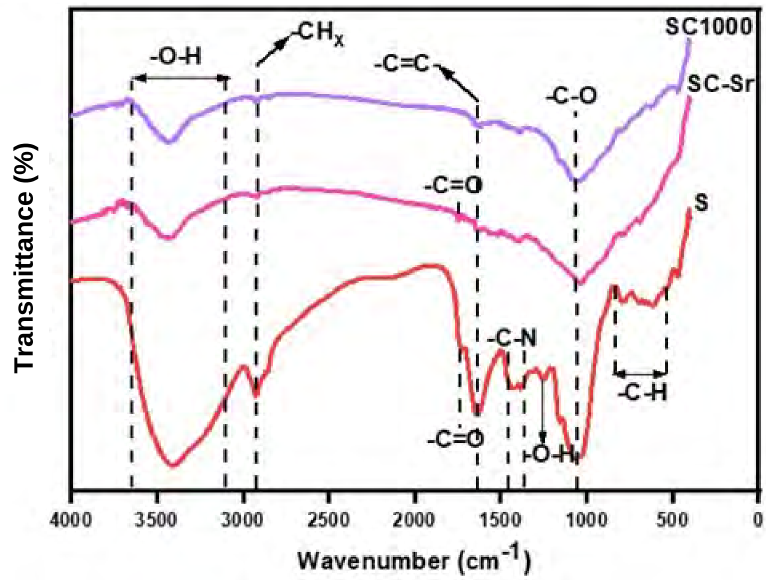

Fig. 4. FT-IR spectra of *R. japonicum* L. (S) and moss-derived biochar (SC1000) and the adsorbed sand moss-derived biochar (SC-Sr)

In the energy spectrum characterization results of XPS elements, the molar ratios of O and N were reduced to varying degrees (Fig. 5). Figure 6 and Table 3 show the results of peak separation of C1s and O1s in the total peak distribution data of XPS. For peak deconvolution of C1s, three values were given: 284.0 to 284.9 eV was peak 1, corresponding to graphite carbon; 285.3 to 286.3eV was peak 2, corresponding to phenols, alcohols, ethers, and carbon in C-N. Peak 3 was 286.5 to 289.3 eV, corresponding to carbonyl, quinine, and ester carbons (Cao *et al.* 2021; Huo *et al.* 2021). The percentage of peak content in Table 4 represents the relative content of atoms with different binding energies of the same element on the material surface. The relative content of peak 1 increased from 57.36% to 62.39%, indicating that high temperature carbonization accelerated the formation of graphite carbon, increased the total content proportion of graphite carbon in functional carbon, and graphite carbon itself was hydrophobic. The increase of graphite carbon and functional carbon ratio after carbonization also increased the hydrophobicity of biochar (Xi *et al.* 2019). In addition, the graphite structure can promote the formation of π-π bonds in the adsorption process of organic molecules, which is beneficial to the chemical adsorption process (Yu *et al.* 2018; Dai *et al.* 2019).

Figures 6b and 6d show the peak separation of O, and Table 3 contains the relative contents of the corresponding surface functional groups. Peak 1 (532.1 to 532.6 eV) corresponds to the oxygen atoms in the carbon group of esters, anhydrides, and oxygen atoms in the -CHO and -CO groups of hydrocarbon groups, and peak 2 (530.4 to 531.9 eV) corresponds to the oxygen atoms of the carbonyl group in quinine (Zhang *et al.* 2018). After carbonization, the relative content of quinine carbonyl oxygen atom in biomass decreases a lot, while the relative content of functional oxygen-containing functional groups on the surface increases, which may enhance the chemisorption behavior of biochar adsorption (Dai *et al.* 2019).

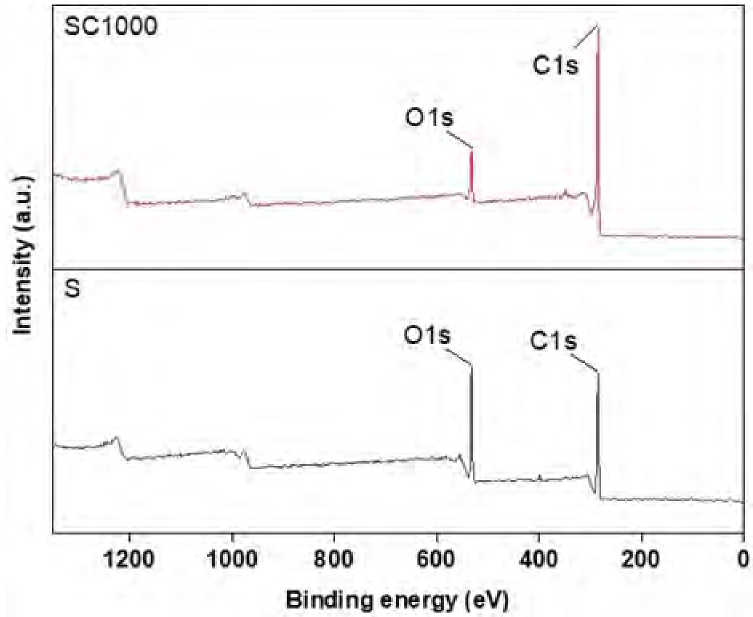

Fig. 5. Full XPS spectrum of *R. japonicum* L. (S) and moss-derived biochar (SC1000)

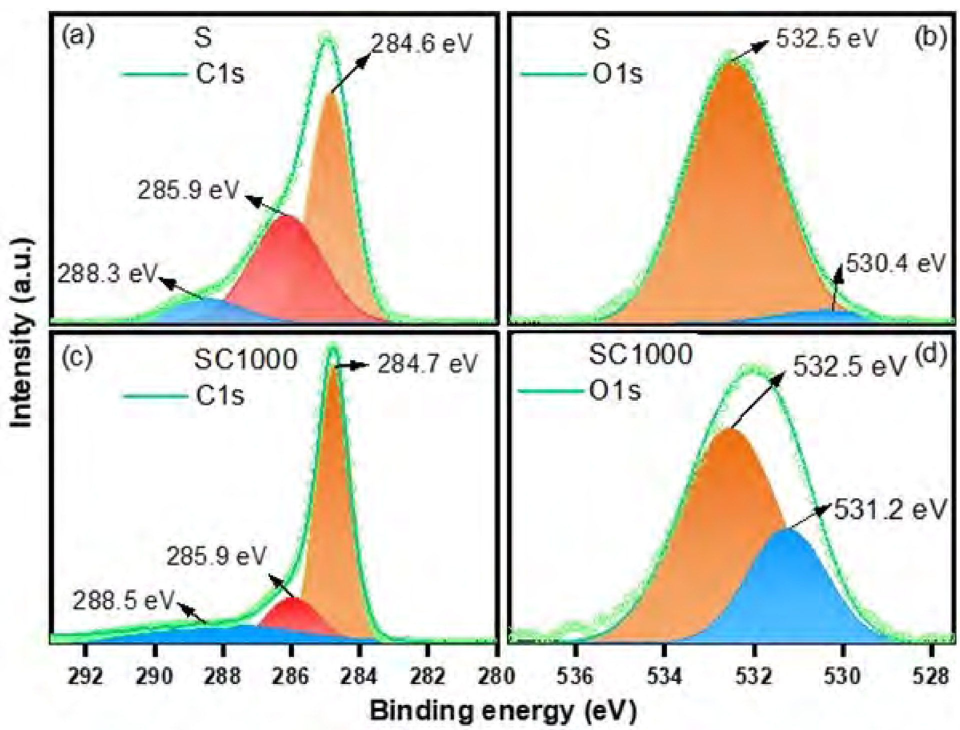

Fig. 6. High resolution C1s and O1s XPS scan of *R. japonicum* L. (S: a, b) and moss-derived biochar (SC1000: c, d)

Table 3. XPS Energy Spectrum Characterization

Adsorbent Type	PP At. (%)				Group Relative Content (%)				
					C1s			O1s	
	C	O	N	S	Peak1	Peak2	Peak3	Peak1	Peak2
S	74.23	22.98	2.47	0.32	57.36	36.85	5.78	95.36	4.64
SC1000	88.86	9.60	1.21	0.33	62.39	15.97	21.64	70.70	29.30

PP At.: The percent mass of each atom;
Group Relative Content (%): The integral area percentage of each binding energy site that was calculated

Sr^{2+} Adsorption Kinetics and Adsorption Isothermal Fitting

The pseudo-first-order and pseudo-second-order kinetic curve fitting of the adsorption kinetics of SC1000 on Sr(II) are shown in Fig. 7. The adsorption was basically stable at 720 min, and the adsorption efficiency of SC1000 on Sr(II) was relatively high before 240 min (Fig. 7). The adsorption model of SC1000 on Sr(II) solution was closer to the pseudo-second-order kinetic model (Table 4, $R^2 > 0.90$). This result indicates that the adsorption process is more likely to be affected by particle diffusion limitation (Hubbe *et al*. 2019).

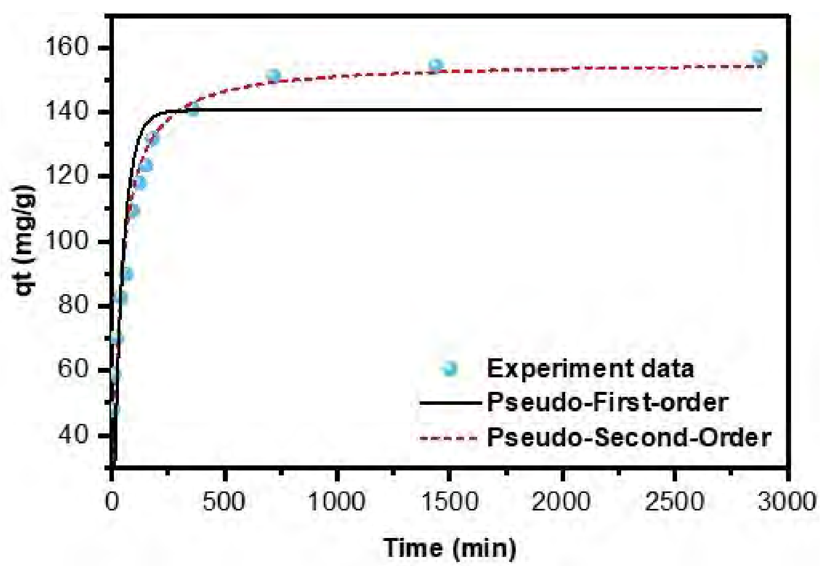

Fig. 7. First- and second-order plots for Sr(II) adsorption onto SC1000; Sr(II) adsorbed onto adsorbent SC1000 at equilibrium (mg/g)(n=3)

Table 4. First-order and Second-order Kinetic Parameters for the Adsorption of Sr(II) onto Sand Moss-derived Biochar (SC1000)

Adsorbent : SC1000	q_e (exp.) (mg/g)	First-order Rate Constants			Second-order Rate Constants		
		K (1/min)	q_e (cal.) (mg/g)	R^2	k_2 (g/mg·min)	q_e (cal.) (mg/g)	R^2
Sr	156.8	0.0232	140.5	0.761	0.000198	155.9	0.906

Before adsorption, the surface of SC1000 was smooth and the pore distribution of the surface structure was obvious (Fig. 8a). After the adsorption of Sr(II) solution, the surface structure of the material was obviously filled, and the material surface presented the phenomenon of film coverage (Fig. 8b). Some visible pores were filled, which made the surface appearance of SC1000 appear dense and smooth after Sr(II) adsorption.

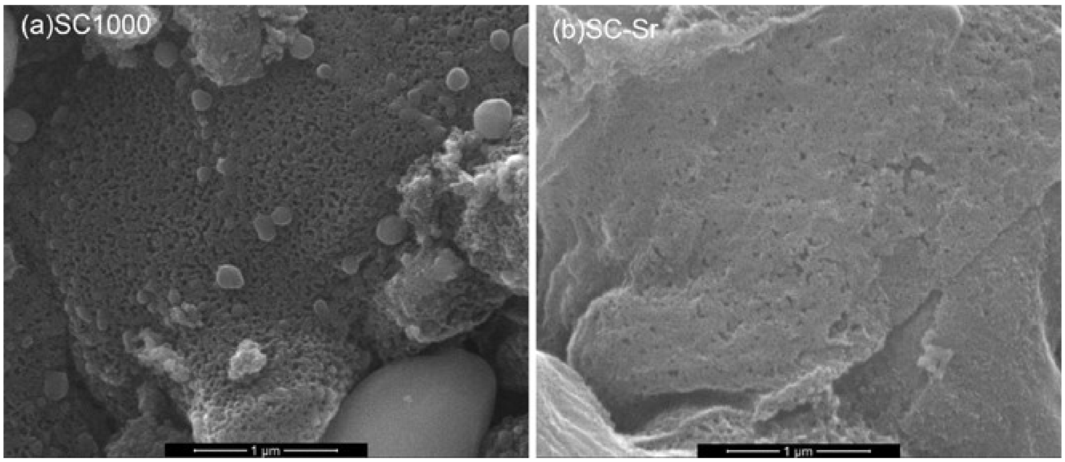

Fig. 8. SEM images of moss-derived biochar before and after Sr adsorption (a: SC1000 and b: SC-Sr)

As shown in Fig. 9, the adsorption of Sr(II) by *R. japonicum* L. carbon was good ($R^2 > 0.90$). The Langmuir model mainly describes the monolayer adsorption process (Tang *et al.* 2018; Yi *et al.* 2021).

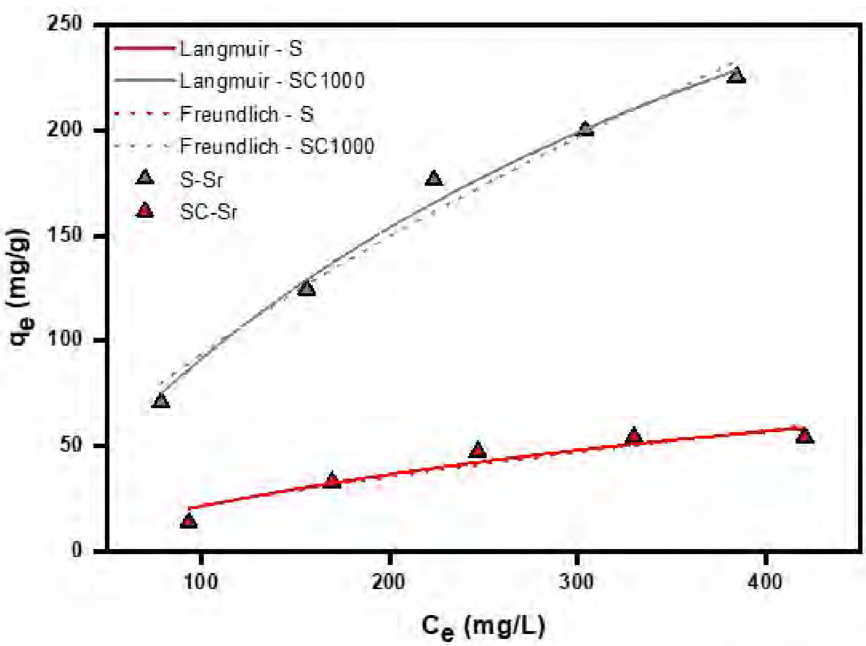

Fig. 9. Adsorption isotherms of different material onto *R. japonicum* L. (S) and moss-derived biochar (SC1000) with q_e amounts of metal adsorbed onto adsorbent (mg/g)(n=3)

Table 5. Langmuir and Freundlich Isotherm Parameters for the Adsorption of Sr(II) on *R. japonicum* L. (S) and Moss-Derived Biochar (SC1000)

Material	Adsorbent	Langmuir Isotherm			Freundlich Isotherm		
		q_{max} (mg/g)	K_L (L/mg)	R^2	K_F (mg/g)	1/*n*	R^2
Sr^{2+}	**S**	129.53	0.00196	0.9192	0.8264	0.7087	0.8866
	SC1000	485.63	0.00232	0.9894	4.1452	0.6768	0.9764

In the adsorption curve, the Langmuir isotherm equation would describe the adsorption type of moss carbon on Sr(II) well, and the theoretical maximum saturated adsorption capacity would be 441 mg/g. In the adsorption behavior analysis of Sr(II), the single-layer adsorption behavior can also better explain the chemical attachment behavior on the material surface as shown in Fig. 9. This is closely related to the functional oxygen-containing functional groups on the surface of the material (Zhu *et al.* 2020). The Freundlich model assumes that the adsorption reaction takes place on the heterogeneous material surface, which occupies a strong adsorption site first, the Freundlich constant parameter 1/*n* is between 0 and 1, indicating the heterogeneity of the adsorbed material surface (Hu *et al.* 2019). The K_F value increased from 0.82 before carbonization to 4.14 after carbonization, indicating that the adsorption capacity of the material increased greatly after treatment. The results showed that the adsorption equilibrium data were consistent with the Langmuir and Freundlich models ($R^2 > 0.94$). In the initial stage of adsorption, the rapid adsorption of micropores was the first, and then the multilayer structure began to fill the mesopore surfaces.

The actual maximum adsorption capacity of Sr(II) obtained in this study was 225 mg/g. Compared with other similar adsorption test reports (as shown in Table 6), the biochar prepared by *R. japonicum* L. achieved the highest adsorption efficiency for Sr(II), indicating the superior metal adsorption performance of moss biochar and its application values. Usually, for biochar that has adsorbed pollutants, the influence of various environmental factors on desorption needs to be considered in consideration of its adsorption stability of pollutants (Zama *et al.* 2017). For instance, biochar will be broken, dissolved, and oxidized after adsorbing heavy metals due to changes in environmental temperature, rainfall, and microbial activities (Wang *et al.* 2020). Therefore, the desorption efficiency for long term application of the biochar needs to be considered in future work.

Table 6. Maximum Adsorption Capacity of Biochar on Sr(II) and Reported in Various Literature

	Work	Adsorbent	Adsorption (mg/g)
Sr^{2+}	Cheng *et al.* (2019)	Mercerized bacterial cellulose membrane	44.86
	Mei *et al.* (2020)	Highly-elastic carboxymethyl chitosan gel	105.81
	Asgari *et al.* (2019)	Nd-BTC metal-organic framework	58.0
	Dan *et al.* (2020)	Silica composites	75.1
	This work	Moss Biochar (SC1000)	225.0

Nd-BTC: Synthesized by Nd ion and benzene tricarboxylic acid with solvothermal method

CONCLUSIONS

1. Biochar was prepared from *R. japonicum* L. by traditional pyrolysis under various conditions. The optimal preparation conditions (1000 °C for 1.5 h) were obtained by analyzing the thermogravimetric properties, yield, structure, and initial adsorption capacity of Sr(II). The specific surface area of biochar obtained under these conditions was 277 m^2/g, and dense mesoporous pores were distributed on the surface. Both FT-IR and XPS characterizations of surface elements and functional groups of biochar showed that the biochar was more favorable for adsorption reaction.
2. At room temperature, the maximum Sr(II) adsorption capacity of moss biochar was 225 mg/g, while the adsorption reaction agreed with quasi-second-order kinetics, Langmuir, and Freundlich isothermal adsorption models. The SEM images show that the adsorbent has a filling effect on the material.

ACKNOWLEDGMENTS

This work was financially supported by the National Key Research and Development Program of China (No. 2020YFE0203200) and the Open Fund Program of the CAS Key Laboratory of Mountain Ecological Restoration and Bioresource Utilization & Ecological Restoration and Biodiversity Conservation Key Laboratory of Sichuan Province, Chengdu Institute of Biology, Chinese Academy of Sciences (No. KXYSWS2204).

REFERENCES CITED

Adamo, P., Giordano, S., Vingiani, S., Cobianchi, R. C., and Violante, P. (2003). "Trace element accumulation by moss and lichen exposed in bags in the city of Naples (Italy)," *Environmental Pollution* 122(1), 91-103. DOI: 10.1016/S0269-7491(02)00277-4

Alshameri, A., He, H., Zhu, J., Xi, Y., Zhu, R., Ma, L., and Tao, Q. (2018). "Adsorption of ammonium by different natural clay minerals: Characterization, kinetics and adsorption isotherms," *Applied Clay Science* 159, 83-93. DOI: 10.1016/j.clay.2017.11.007

Anukam, A., Mamphweli, S., Reddy, P., Okoh, O., and Meyer, E. (2015). "An investigation into the impact of reaction temperature on various parameters during torrefaction of sugarcane bagasse relevant to gasification," *Journal of Chemistry* 2015, article ID 235163. DOI: 10.1155/2015/235163

Asgari, P., Mousavi, S. H., Aghayan, H., Ghasemi, H., and Yousefi, T. (2019). "Nd-BTC metal-organic framework (MOF); synthesis, characterization and investigation on its adsorption behavior toward cesium and strontium ions," *Microchemical Journal* 150, article ID 104188. DOI: 10.1016/j.microc.2019.104188

Barquilha, C. E. R., and Braga, M. C. B. (2021). "Adsorption of organic and inorganic pollutants onto biochars: Challenges, operating conditions, and mechanisms," *Bioresource Technology Reports* 15, article ID 100728. DOI: 10.1016/j.biteb.2021.100728

Burger, A., and Lichtscheidl, I. (2019). "Strontium in the environment: Review about reactions of plants towards stable and radioactive strontium isotopes," *Science of The Total Environment* 653, 1458-1512. DOI: 10.1016/j.scitotenv.2018.10.312

Cao, X., Li, Z., Chen, H., Zhang, C., Zhang, Y., Gu, C., Xu, X., and Li, Q. (2021). "Synthesis of biomass porous carbon materials from bean sprouts for hydrogen evolution reaction electrocatalysis and supercapacitor electrode," *International Journal of Hydrogen Energy* 46(36), 18887-18897. DOI: 10.1016/j.ijhydene.2021.03.038

Cha, J. S., Park, S. H., Jung, S., Ryu, C., Jeon, J., Shin, M., and Park, Y. (2016). "Production and utilization of biochar: A review," *Journal of Industrial and Engineering Chemistry* 40, 1-15. DOI: 10.1016/j.jiec.2016.06.002

Cheng, R., Kang, M., Zhuang, S., Shi, L., Zheng, X., and Wang, J. (2019). "Adsorption of Sr(II) from water by mercerized bacterial cellulose membrane modified with EDTA," *Journal of Hazardous Materials* 364, 645-653. DOI: 10.1016/j.jhazmat.2018.10.083

Choi, Y., Choi, T., Gurav, R., Bhatia, S. K., Park, Y., Kim, H. J., Kan, E., and Yang, Y. (2020). "Adsorption behavior of tetracycline onto *Spirulina* sp. (microalgae)-derived biochars produced at different temperatures," *Science of The Total Environment* 710, article ID 136282. DOI: 10.1016/j.scitotenv.2019.136282

Dai, Y., Zhang, N., Xing, C., Cui, Q., and Sun, Q. (2019). "The adsorption, regeneration and engineering applications of biochar for removal organic pollutants: A review," *Chemosphere* 223, 12-27. DOI: 10.1016/j.chemosphere.2019.01.161

Dan, H., Ding, Y., Wang, E., Yang, W., He, X., Chen, L., Xian, Q., Yi, F., and Zhu, W. (2020). "Manganese dioxide-loaded mesoporous SBA-15 silica composites for effective removal of strontium from aqueous solution," *Environmental Research* 191, article ID 110040. DOI: 10.1016/j.envres.2020.110040

Deng, J., Xiong, T., Wang, H., Zheng, A., and Wang, Y. (2016). "Effects of cellulose, hemicellulose, and lignin on the structure and morphology of porous carbons," *ACS Sustainable Chemistry & Engineering* 4(7), 3750-3756. DOI: 10.1021/acssuschemeng.6b00388

Espiñeira, J. M., Uzal, E. N., Gómez Ros, L. V., Carrión, J. S., Merino, F., Ros Barceló, A., and Pomar, F. (2011). "Distribution of lignin monomers and the evolution of lignification among lower plants," *Plant Biology* 13(1), 59-68. DOI: 10.1111/j.1438-8677.2010.00345.x

Ezzati, R. (2020). "Derivation of pseudo-first-order, pseudo-second-order and modified pseudo-first-order rate equations from Langmuir and Freundlich isotherms for adsorption," *Chemical Engineering Journal* 392, article ID 123705. DOI: 10.1016/j.cej.2019.123705

Hu, Y., Zhu, Y., Zhang, Y., Lin, T., Zeng, G., Zhang, S., Wang, Y., He, W., Zhang, M., and Long, H. (2019). "An efficient adsorbent: Simultaneous activated and magnetic ZnO doped biochar derived from camphor leaves for ciprofloxacin adsorption," *Bioresource Technology* 288, article ID 121511. DOI: 10.1016/j.biortech.2019.121511

Hubbe, M., Azjzja , S., and Douven, S. (2019). "Implications of apparent pseudo-second-order adsorption kinetics onto cellulosic materials: A review," *BioResources* 14(3), 7582-7626. DOI: 10.15376/biores.14.3.7582-7626

Huff, M. D., Kumar, S., and Lee, J. W. (2014). “Comparative analysis of pinewood, peanut shell, and bamboo biomass derived biochars produced *via* hydrothermal conversion and pyrolysis,” *Journal of Environmental Management* 146, 303-308. DOI: 10.1016/j.jenvman.2014.07.016

Huo, J., Yu, G., and Wang, J. (2021). “Adsorptive removal of Sr(II) from aqueous solution by polyvinyl alcohol/graphene oxide aerogel,” *Chemosphere* 278, article ID 130492. DOI: 10.1016/j.chemosphere.2021.130492

Jian, X., Zhuang, X., Li, B., Xu, X., Wei, Z., Song, Y., and Jiang, E. (2018). “Comparison of characterization and adsorption of biochars produced from hydrothermal carbonization and pyrolysis,” *Environmental Technology & Innovation* 10, 27-35. DOI: 10.1016/j.eti.2018.01.004

Kadam, A., Saratale, R. G., Shinde, S., Yang, J., Hwang, K., Mistry, B., Saratale, G. D., Lone, S., Kim, D., Sung, J., *et al.* (2019). “Adsorptive remediation of cobalt oxide nanoparticles by magnetized α-cellulose fibers from waste paper biomass,” *Bioresource Technology* 273, article ID 386-393. DOI: 10.1016/j.biortech.2018.11.041

Kim, J. E., Bhatia, S. K., Song, H. J., Yoo, E., Jeon, H. J., Yoon, J., Yang, Y., Gurav, R., Yang, Y., Kim, H. J., *et al.* (2020). “Adsorptive removal of tetracycline from aqueous solution by maple leaf-derived biochar,” *Bioresource Technology* 306, article ID 123092. DOI: 10.1016/j.biortech.2020.123092

Lawal, A. A., Hassan, M. A., Zakaria, M. R., Yusoff, M. Z. M., Norrrahim, M. N. F., Mokhtar, M. N., and Shirai, Y. (2021). “Effect of oil palm biomass cellulosic content on nanopore structure and adsorption capacity of biochar,” *Bioresource Technology* 332, article ID 125070. DOI: 10.1016/j.biortech.2021.125070

Li, X., Xu, Q., Fu, Y., and Guo, Q. (2014), "Preparation and characterization of activated carbon from Kraft lignin *via* KOH activation," *Environmental Progress & Sustainabl e Energy* 33(2), 519-526. DOI: 10.1002/ep.11794

Li, Y., Yu, H., Liu, L., and Yu, H. (2021). “Application of co-pyrolysis biochar for the adsorption and immobilization of heavy metals in contaminated environmental substrates,” *Journal of Hazardous Materials* 420, article ID 126655. DOI: 10.1016/j.jhazmat.2021.126655

Liu, Y., Wang, P., Gojenko, B., Yu, J., Wei, L., Luo, D., and Xiao, T. (2021). “A review of water pollution arising from agriculture and mining activities in Central Asia: Facts, causes and effects,” *Environmental Pollution* 291, article ID 118209. DOI: 10.1016/j.envpol.2021.118209

Llaurado, J. G. (2011). “Handbook of environmental engineering: Vol. 11 Environmental bioengineering,” *Management of Environmental Quality* 22(4). DOI: 10.1108/meq.2011.08322daa.009

Ly, Q. V., Hu, Y., Li, J., Cho, J., and Hur, J. (2019). “Characteristics and influencing factors of organic fouling in forward osmosis operation for wastewater applications: A comprehensive review,” *Environment International* 129, 164-184. DOI: 10.1016/j.envint.2019.05.033

Mei, J., Mo, S., Zhang, H., Zheng, X., and Li, Z. (2020). “Removal of Sr(II) from water with highly-elastic carboxymethyl chitosan gel,” *International Journal of Biological Macromolecules* 163, 1097-1105. DOI: 10.1016/j.ijbiomac.2020.07.038

Nagata, T. (2019). “Effect of strontium on the growth, ion balance, and suberin induction in *Solanum lycopersicum*,” *Plant Root* 13, 9-14. DOI: 10.3117/plantroot.13.9

Oginni, O., and Tingi, K. (2020). "Influence of high carbonization temperatures on microstructural and physicochemical characteristics of herbaceous biomass derived biochars," *Journal of Environmental Chemical Engineering* 8(5), article ID 104169. DOI: 10.1016/j.jece.2020.104169

Oliveira, F. R., Patel, A. K. P., Jaisi, D. P., Adhikari, S., Lu, H., and Kumar, S. K. (2017). "Environmental application of biochar: Current status and perspectives," *Bioresource Technology* 246, 110-122. DOI: 10.1016/j.biortech.2017.08.122

Plank, N. (1946). "The nature of cellulose in *Sphagnum*," *American Journal of Botany* 33(5), 335-337. DOI: 10.2307/2437120

Reza, M. T., Uddin, M. H., Lynam, J. G., and Coronella, C. J. (2014). "Engineered pellets from dry torrefied and HTC biochar blends," *Biomass and Bioenergy* 63, 229-238. DOI: 10.1016/j.biombioe.2014.01.038

Saber, S. E. M., Rahim, S. B. A., Wan, Y. H., Olalere, O. A., and Habeeb, O. A. (2019). "Morphological, thermal stability and textural elucidation of raw and activated palm kernel shell and their potential use as environmental-friendly adsorbent," *Chemical Data Collections* 21: 100235. DOI: 10.1016/j.cdc.2019.100235

Saha, N., Saba, A., and Reza, M. T. (2019). "Effect of hydrothermal carbonization temperature on pH, dissociation constants, and acidic functional groups on hydrochar from cellulose and wood," *Journal of Analytical and Applied Pyrolysis* 137, 138-145. DOI: 10.1016/j.jaap.2018.11.018

Schwanninger, M., Rodrigues, J. C., Pereira, H., and Hinterstoisser, B. (2004). "Effects of short-time vibratory ball milling on the shape of FT-IR spectra of wood and cellulose," *Vibrational Spectroscopy* 36(2004), 23-40. DOI: 10.1016/j.vibspec.2004.02.003

Stanković, J. D., Sabovljević, A. D., and Sabovljević, M. S. (2018). "Bryophytes and heavy metals: A review," *Acta Botanica Croatica* 77(2), 109-118. DOI: 10.2478/botcro-2018-0014

Steinhauser, G., Brandl, A., and Johnson, T. E. (2014). "Comparison of the Chernobyl and Fukushima nuclear accidents: A review of the environmental impacts," *Science of The Total Environment* 470-471(2014), 800-817. DOI: 10.1016/j.scitotenv.2013.10.029

Subratti, A., Vidal, J. L., Lalgee, L. J., Kerton, F. M., and Jalsa, N. K. (2021). "Preparation and characterization of biochar derived from the fruit seed of *Cedrela odorata* L. and evaluation of its adsorption capacity with methylene blue," *Sustainable Chemistry and Pharmacy* 21, article ID 100421. DOI: 10.1016/j.scp.2021.100421

Tang, L., Yu, J., Pang, Y., Zeng, G., Deng, Y., Wang, J., Ren, X., Ye, S., Peng, B., and Feng, H. (2018). "Sustainable efficient adsorbent: Alkali-acid modified magnetic biochar derived from sewage sludge for aqueous organic contaminant removal," *Chemical Engineering Journal* 336, 160-169. DOI: 10.1016/j.cej.2017.11.048

Tripathi, M., Sahu, J. N., and Ganesan, P. (2016). "Effect of process parameters on production of biochar from biomass waste through pyrolysis: A review," *Renewable and Sustainable Energy Reviews* 55(2016), 467-481. DOI: 10.1016/j.rser.2015.10.122

Uchimiya, M., Wartelle, L. H., Klasson, K. T., Fortier, C. A., and Lima, I. M. (2011). "Influence of pyrolysis temperature on biochar property and function as a heavy metal sorbent in soil," *Journal of Agricultural and Food Chemistry* 59(6), 2501-2510. DOI: 10.1021/jf104206c

Wang, L., O, C, D., Rinklebe, J., Ok, Y, S., Tsang, D, C, W., Shen, Z., Hou, D. (2020). "Biochar aging: Mechanisms, physicochemical changes, assessment, and implications for field applications," *Environmental Science & Technology* 54(23), 14797-14814. DOI: 10.1021/acs.est.0c04033

Wyatt, H. D. M., Ashton, N. W., and Dahms, T. E. S. (2008). "Cell wall architecture of *Physcomitrella patens* is revealed by atomic force microscopy," *Botany* 86(4), 385-397. DOI: 10.1139/B08-003

Xi, X., Jiang, S., Zhang, W., Wang, K., Shao, H., and Wu, Z. (2019). "An experimental study on the effect of ionic liquids on the structure and wetting characteristics of coal," *Fuel* 244, 176-183. DOI: 10.1016/j.fuel.2019.01.183

Xu, Z., Xiang, Y., Zhou, H., Yang, J., He, Y., Zhu, Z., and Zhou, Y. (2021). "Manganese ferrite modified biochar from vinasse for enhanced adsorption of levofloxacin: Effects and mechanisms," *Environmental Pollution* 272, article ID 115968. DOI: 10.1016/j.envpol.2020.115968

Yao, B., Luo, Z., Du, S., Yang, J., Zhi, D., and Zhou, Y. (2021). "Sustainable biochar/MgFe2O4 adsorbent for levofloxacin removal: Adsorption performances and mechanisms," *Bioresource Technology* 340, article ID 125698. DOI: 10.1016/j.biortech.2021.125698

Yi, Y., Tu, G., Ying, G., Fang, Z., and Tsang, E. P. (2021). "Magnetic biochar derived from rice straw and stainless steel pickling waste liquor for highly efficient adsorption of crystal violet," *Bioresource Technology* 341, article ID 125743. DOI: 10.1016/j.biortech.2021.125743

Yiin, C. L., Yusup, S., Quitain. A. T., Uemura, Y., Sasaki, M., and Kida, T. (2018). "Thermogravimetric analysis and kinetic modeling of low-transition-temperature mixtures pretreated oil palm empty fruit bunch for possible maximum yield of pyrolysis oil," *Bioresource Technology* 255, 189-197. DOI: 10.1016/j.biortech.2018.01.132

Yoshikawa, K., Overduin, P. P., and Harden, J. W. (2004). "Moisture content measurements of moss (*Sphagnum* spp.) using commercial sensors," *Permafrost and Periglacial Processes* 15(4), 309-318. DOI: 10.1002/ppp.505

Yu, W., Lian, F., Cui, G., and Liu, Z. (2018). "N-doping effectively enhances the adsorption capacity of biochar for heavy metal ions from aqueous solution," *Chemosphere* 193, 8-16. DOI: 10.1016/j.chemosphere.2017.10.134

Zama, E. F., Zhu. Y, G., Reid, B, J., and Sun, G, X. (2017). "The role of biochar properties in influencing the sorption and desorption of Pb(II), Cd(II) and As(III) in aqueous solution," *Journal of Cleaner Production* 148, 127-136. DOI: 10.1016/j.jclepro.2017.01.125

Zamora-Ledezma, C., Negrete-Bolagay, D., Figueroa, F., Zamora-Ledezma, E., Ni, M., Alexis, F., and Guerrero, V. H. (2021). "Heavy metal water pollution: A fresh look about hazards, novel and conventional remediation methods," *Environmental Technology & Innovation* 22, article ID 101504. DOI: 10.1016/j.eti.2021.101504

Zhang, J., Liu, J., and Liu, R. (2015a). "Effects of pyrolysis temperature and heating time on biochar obtained from the pyrolysis of straw and lignosulfonate," *Bioresource Technology* 176, 288-291. DOI: 10.1016/j.biortech.2014.11.011

Zhang, J., Liu, J., and Liu, R. (2015b). "Effects of pyrolysis temperature and heating time on biochar obtained from the pyrolysis of straw and lignosulfonate," *Bioresource Technology* 176, 288-291. DOI: 10.1016/j.biortech.2014.11.011

Zhang, S., Lyu, H., Tang, J., Song, B., Zhen, M., and Liu, X. (2018). "A novel biochar supported CMC stabilized nano zero-valent iron composite for hexavalent chromium removal from water," *Chemosphere* 217, 686-694. DOI: 10.1016/j.chemosphere.2018.11.040

Zhu, L., Shen, D., and Luo, K. H. (2020). "A critical review on VOCs adsorption by different porous materials: Species, mechanisms and modification methods," *Journal of Hazardous Materials* Article ID 122102. DOI: 10.1016/j.jhazmat.2020. 122102

Article submitted: January 16, 2022; Peer review completed: April 25, 2022; Revised version received: May 1, 2022; Accepted: May 2, 2022; Published: May 6, 2022.
DOI: 10.15376/biores.17.3.3965-3983